

Synthesis, Properties, and Application as Emitters in Organic Electroluminescence Devices of Quinacridone- and Squarylium-Dye-Centred Dendrimers

Masaki Matsui,*[1] Saori Tanaka,[1] Kazumasa Funabiki,[1] and Toru Kitaguchi[2]

[1]Department of Materials Science and Technology, Faculty of Engineering, Gifu University, Yanagido, Gifu 501-1193

[2]Daicel Chemical Industries, Ltd., 1239 Shinzaike, Aboshi-ku, Himezi 671-1283

Received August 17, 2005; E-mail: matsui@apchem.gifu-u.ac.jp

The UV–vis absorption and fluorescence spectra, solubility, and application as emitters in single-layer organic electroluminescence (EL) devices of novel quinacridone- and squarylium-dye-centred dendrimers (**G$_n$-QAs** and **G$_n$-SQs**) were examined. The respective dendrimers showed no remarkable differences in the UV–vis absorption (λ_{max}) and photoluminescence (PL) maxima (λ_{em}). The solubility of dendrimers drastically increased at higher generation. The EL maxima of **G$_n$-QAs** and **G$_n$-SQs** were observed at 522 and 710 nm, respectively. In the case of **G$_n$-QAs**, the EL intensity under the fixed bias voltage decreased at higher generation due to a decrease in energy transfer from the host molecules to **QA**. Meanwhile, in the case of **G$_n$-SQs**, the EL intensity increased upon higher generation because of increased current density and the improvement of concentration quenching.

Dye-centred dendrimers have attracted much attention due to their functionalities. Azo-,[1] xanthene-,[2] porphyrin-,[3] and phthalocyanine-centred dendrimers[4] have been reported to show unique properties. Meanwhile, **QA**[5–7] and **SQ**[8,9] can act as emitters in EL devices. In our previous paper, 6-substituted 2,3-dicyano-5-[4-(diethylamino)styryl]-7-methyl-6*H*-1,4-diazepines, which act as emitters in EL devices, were found to increase EL intensity under fixed bias voltage.[10] We thought that much more bulky dye-centred dendrimers may act as good emitters. Perylene-3,4:9,10-tetracarboxylic diimides having polyphenylene dendrons in the bay positions have been reported to show a red-orange emission in single-layer EL devices.[11] Naphthalimide-centred dendrimers attached with hole- and electron-transport dendrons[12] and coumarin-centred dendrimers having hole-transport triarylamine dendrons[13] have been examined as emitters in single-layer EL devices. We report herein the synthesis, UV–vis absorption and fluorescence spectra, and solubility of **G$_n$-QAs** and **G$_n$-SQs**, and their application as emitters in single-layer EL devices.

Results and Discussion

Synthesis of G$_n$-QAs and G$_n$-SQs. **G$_n$-QAs** and **G$_n$-SQs** were synthesized as shown in Scheme 1. **G$_n$-QAs** were prepared by the reaction of **QA** (**1**) with dendrons **G$_n$-Br** in moderate to good yields. The dihydroxy **SQ** dye **2** reacted with **G$_n$-Br** to give **G$_n$-SQs** in low to moderate yields.

Figure 1 shows the ^{1}H NMR spectra of **G$_n$-QAs**. Proton peaks attributed to **QA** nuclei c, a, b, d, and e were observed at around 7.1, 7.3, 7.6, 8.5, and 8.7 ppm, respectively. *t*-Butyl protons were observed at around 1.2 ppm. Methylene protons i, f′, and f″ were observed at around 4.9 ppm. Interestingly, the intensity of methylene protons f adjacent to a **QA** nuclei observed at around 5.7 ppm decreased at higher generation. The aromatic protons g, g′, g″, h, h′, and h″ were observed at around 6.7 ppm. The peripheral aromatic protons j and k were observed at around 7.3 and 7.4 ppm, respectively.

The ^{1}H NMR spectra of **G$_n$-SQs** are shown in Fig. 2. *N*-Butyl protons were observed at 1.0, 1.3, 1.4, and 4.0 ppm. Methine protons a in the central **SQ** moiety were observed at 5.8 ppm. Benzothiazolyl protons b, d, and c were observed at around 6.7, 6.8, and 7.3 ppm, respectively. A singlet *t*-butyl proton peak was observed at 1.3 ppm. Methylene protons f, f′, f″, and i were observed at around 5.0 ppm. The aromatic protons g, g′, g″, h, h′, and h″ were observed at around 6.7 ppm. The peripheral aromatic protons j and k were observed at around 7.2 and 7.4 ppm, respectively.

UV–Vis Absorption and Fluorescence Spectra. Figure 3 show the UV–vis absorption and fluorescence spectra of **G$_n$-QAs** and **G$_n$-SQs** in chloroform. The λ_{max} were observed at 482 and 514 nm with a shoulder peak at around 450 nm. The molar absorption coefficients ε at around 482 and 514 nm were calculated to be 10300 to 11300 and 17800 to 19900, respectively, there being no marked difference among **G$_n$-QAs**. This result indicates that the planarity of the **QA** skeleton is not affected by the dendrons. The λ_{em} were observed at 531 and 586 nm.

The λ_{max} of **G$_n$-SQs** were observed at 685 nm, there being no remarkable difference among **G$_n$-SQs**. The ε value slightly decreased at higher generation in the range of 209000 to 271000, probably due to twisting of the central **SQ** dye by surrounding bulky dendrons. The λ_{em} were observed at around 698 nm.

Solubility. The solubility of **G$_n$-QAs** and **G$_n$-SQs** in cyclohexane at 25 °C is shown in Table 1. It is surprising that **SQ** and **QA** are soluble in cyclohexane. The solubility of **G$_n$-QAs** and **G$_n$-SQs** drastically increased as generation was increased. The melting points of **G$_n$-SQ** and **G$_n$-QA** became lower with increasing generation. This result indicates that the intermolecu-

Published on the web January 13, 2006; DOI 10.1246/bcsj.79.170

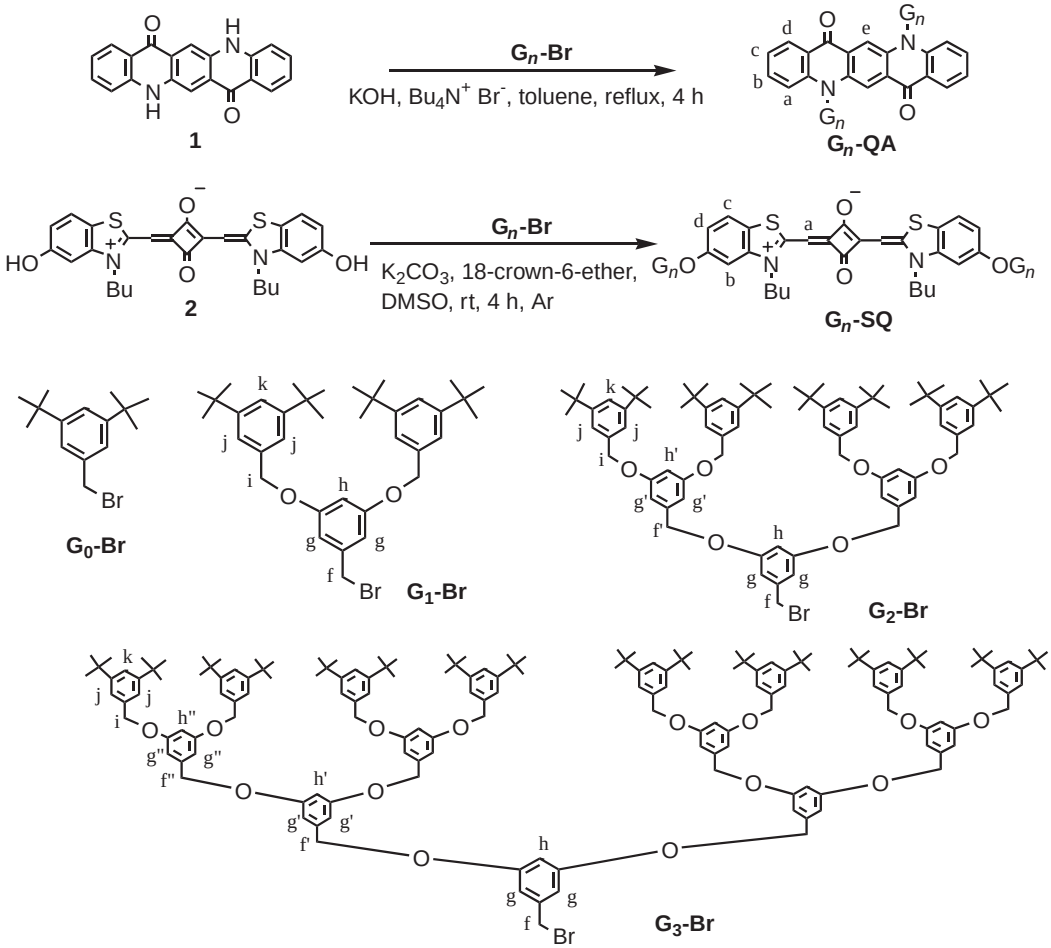

Scheme 1.

lar interactions between the central dye molecules are prevented by introducing bulky dendrons to increase the solubility.

Concentration-Quenching. The relationship between the fluorescence intensity and concentration of **G_n-QAs** and **G_n-SQs** are shown in Fig. 4. At higher concentrations of **G_n-QAs** and **G_n-SQs**, the fluorescence intensity increased, reached a maximum point, and then decreased. The maximum concentrations for **G_0-**, **G_1-**, **G_2-**, and **G_3-QAs** were observed at 4×10^{-5} mol dm^{-3}, there being no effect of dendrons on concentration-quenching. Meanwhile, those for **G_0-**, **G_1-**, **G_2-**, and **G_3-SQs** were observed at 2×10^{-6}, 3×10^{-6}, 4×10^{-6}, and 4×10^{-6} mol dm^{-3}, respectively. The melting points of **G_n-SQs** in the respective generation were lower than those of **G_n-QAs** as shown in Table 1. **G_n-SQs** were more soluble than **G_n-QAs** in cyclohexane. These results suggest that the intermolecular interactions in **G_n-SQs** are less than those in **G_n-QAs**, which results in an improvement in concentration-quenching.

Emitters in EL Devices. A single-layer organic electroluminescence device prepared is shown in Fig. 5.

The EL spectra of **G_n-QAs** and **G_n-SQs** are shown in Fig. 6. The EL maxima of **G_n-QAs** were observed at 522 nm together with an emission around 430 nm. Those of **G_n-SQs** were observed at 710 nm.

The relationship between the EL intensity and bias voltage of **G_n-QAs** and **G_n-SQs** is shown in Fig. 7. In the case of **G_n-QAs**, at higher generation, the EL intensity under the fixed bias voltage decreased. Meanwhile, in the case of **G_n-SQs**, the EL intensity increased at higher generation.

Figure 8 shows the *I–V* characteristics of **G_n-QAs** and **G_n-SQs**. In the case of **G_n-QAs**, no remarkable change in turn-on voltage was observed. Meanwhile, in the case of **G_n-SQs**, the turn-on voltage was lower upon higher generation.

Figure 9 shows the relationship between the EL intensity and current density of **G_n-QAs** and **G_n-SQs**. In the case of **G_n-QAs**, the EL intensity under the fixed current density decreased at higher generation. The slope of the line at the origin represents the EL efficiency. The EL efficiency of **G_n-QAs** decreased upon higher generation. This result indicates that the concentration quenching of **G_n-QAs** does not contribute to an improvement of EL intensity. Meanwhile, in the case of **G_n-SQs**, the EL intensity under the fixed current density increased at higher generation. The EL efficiency of **G_n-SQs** also increased as generation was increased, indicating that the improvement of concentration quenching was effective to increase EL intensity.

G_n-QAs doped in PVK/PBD film showed an absorption band in the range of 400 to 550 nm, in which the PL band from PVK/PBD at around 430 nm was observed. Even when the amount of **G_0-QA** was increased from 1.35×10^{-7} to $9.19 \times$

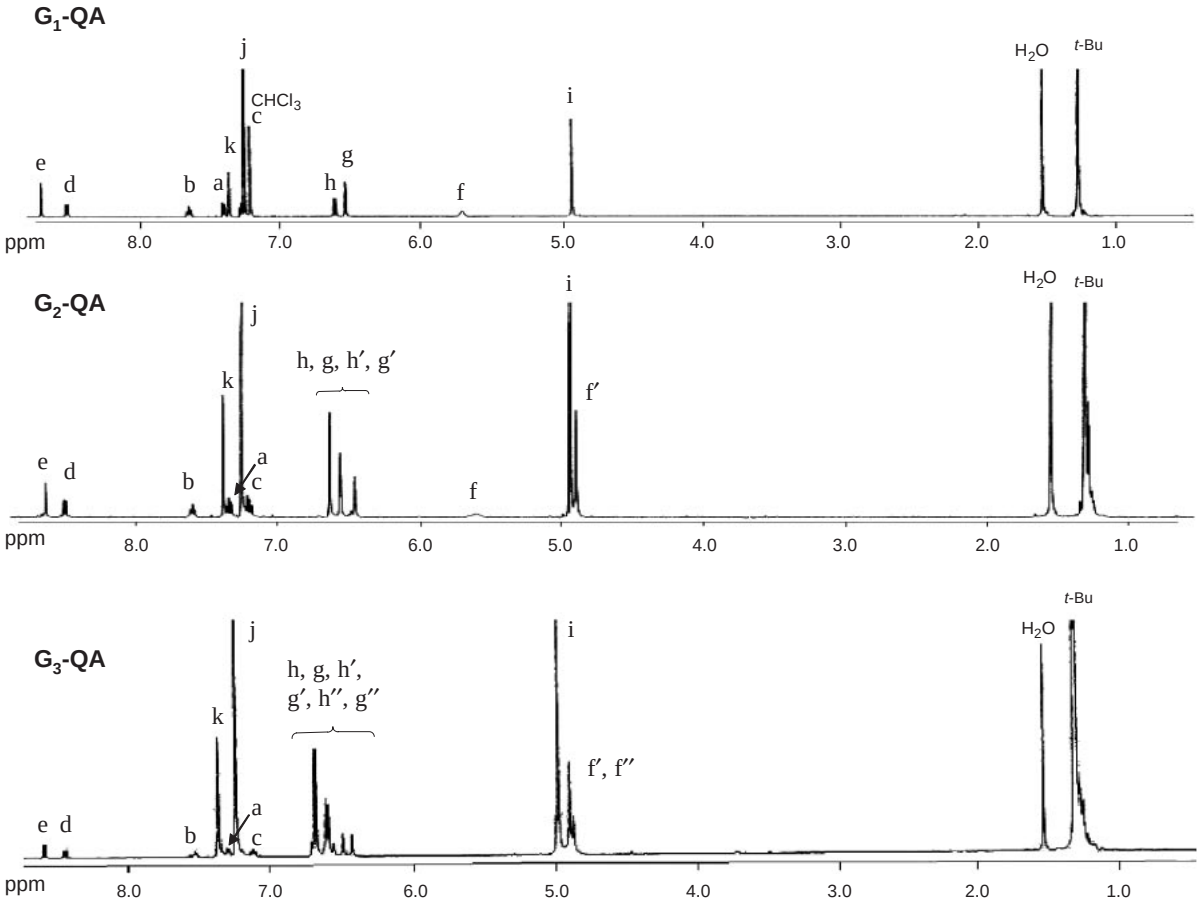

Fig. 1. ^{1}H NMR spectra of **G$_n$-QAs**.

Table 1. Physical Properties of **G$_n$-QAs** and **G$_n$-SQs**

Compd	mp/°C	λ_{max}[a)]/nm	λ_{em}[a)]/nm	Solubility[b)] /mmol dm^{-3}
G$_0$-QA	>300	483 (10300), 516 (17800)	533, 567	0.57
G$_1$-QA	>300	482 (10400), 514 (18100)	531, 566	0.75
G$_2$-QA	112–113	481 (11300), 513 (19900)	531, 565	16
G$_3$-QA	102–103	482 (10900), 514 (19100)	530, 565	>30
G$_0$-SQ	>300	684 (271000)	698	0.042
G$_1$-SQ	126–127	684 (252000)	697	21
G$_2$-SQ	74–76	685 (215000)	697	43
G$_3$-SQ	44–45	685 (209000)	697	>60

a) Measured in chloroform (**G$_n$-QAs**: 5×10^{-5} mol dm^{-3}, **G$_n$-SQs**: 5×10^{-6} mol dm^{-3}) at 25 °C. The emission spectra were measured by irradiating 514 nm light for **G$_n$-QAs** and 684 nm light for **G$_n$-SQs**, respectively. b) Measured in cyclohexane at 25 °C.

10^{-7} mol, no remarkable change in current density was observed. These results indicate that **G$_n$-QAs** are mainly excited by energy transfer from host PVK/PBD.

G$_n$-SQs showed a UV–vis absorption band in the range of 560 to 740 nm, there being no absorption around 430 nm. When the amount of **G$_0$-SQ** increased from 1.3×10^{-7} to 3.3×10^{-7} mol, the current density increased. These results indicate that **G$_n$-SQs** are mainly excited by a carrier-trap mechanism. Therefore, the decrease in EL intensity of **G$_n$-QAs** in higher generation under the fixed bias voltage could be attributed to inhibition of energy transfer from PVK/PBD to **QA** due to bulky dendrons. Actually, the fluorescence around 430 nm increased as the generation was increased as shown in Fig. 6a. The EL intensity of **G$_n$-SQs** under the fixed bias voltage was larger as higher was the generation as shown in Fig. 7b. This can be attributed to increased current density under the fixed bias voltage and the improvement of concentration quenching of **G$_n$-SQs**.

Conclusion

G$_n$-QAs and **G$_n$-SQs** showed λ_{max} at around 515 and 685 nm in chloroform, respectively. The λ_{em} of these dendrimers

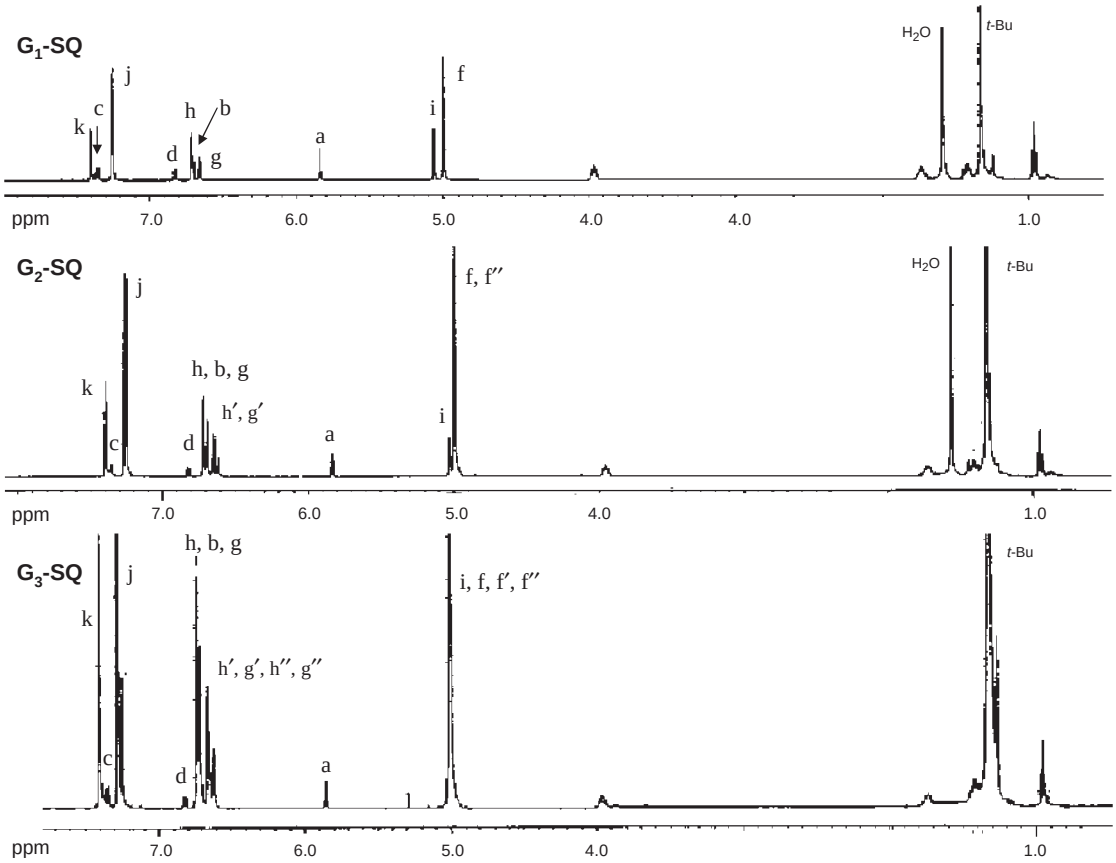

Fig. 2. ^{1}H NMR spectra of **G$_n$-SQs**.

were observed at around 531 and 697 nm, respectively. The solubility of **G$_n$-QAs** and **G$_n$-SQs** drastically increased as the generation was increased. **G$_n$-QAs** and **G$_n$-SQs** showed EL maxima at 522 and 710 nm, respectively. The EL intensity of **G$_n$-QAs** decreased at higher generation due to inhibition of energy transfer from host PVK/PBD. Meanwhile, the EL intensity of **G$_n$-SQs** under the fixed bias voltage increased upon higher generation due to increased current density.

Experimental

Instruments. Melting points were measured with a Yanagimoto MP-52 micro-melting-point apparatus. NMR spectra were obtained by a Varian Inova 500 spectrometer. EIMS spectra were measured with a JEOL MStation 700 spectrometer. UV–vis absorption and fluorescence spectra were taken on Hitachi U-3500 and F-4500 spectrophotometers, respectively. Elemental analysis was performed with a Yanaco MT-6 CHN corder.

Materials. 5-Hydroxy-2-methylbenzothiazole, butyl iodide, squaric acid, and quinacridone (**1**) were purchased from Tokyo Kasei Co., Ltd. 3,5-Dihydroxybenzyl alcohol was purchased from Sigma-Aldrich Co., Ltd. 3,5-Di-*t*-butylbenzyl bromide (**G$_0$-Br**), **G$_1$-Br**, **G$_2$-Br**, and **G$_3$-Br** were synthesized as described in the literature.[14] **G$_0$-SQ** was synthesized as described in the literature.[15]

Synthesis of G$_n$-QAs. To a toluene solution (**G$_0$**, **G$_1$**, **G$_2$**: 20 cm^3, **G$_3$**: 10 cm^3) of quinacridone (**1**) (**G$_0$**, **G$_1$**, **G$_2$**: 31 mg (0.1 mmol), **G$_3$**: 16 mg (0.05 mmol)) and tetrabutylammonium bromide (**G$_0$**, **G$_1$**, **G$_2$**: 31 mg (0.1 mmol), **G$_3$**: 16 mg (0.05 mmol)), and 37.5% aqueous potassium hydroxide (**G$_0$**, **G$_1$**, **G$_2$**: 1.4 cm^3, **G$_3$**: 0.7 cm^3) was added **G$_n$-Br** (**G$_0$**, **G$_1$**, **G$_2$**: 0.25 mmol, **G$_3$**: 0.13 mmol). The mixture was refluxed for 4 h. After the reaction was completed, the solvent was evaporated. Water (50 cm^3) was added to the mixture. The product was extracted with dichloromethane (50 cm^3 × 3), purified by column chromatography (**G$_0$**: SiO_2, CH_2Cl_2, **G$_1$**: SiO_2, CH_2Cl_2:C_6H_{14} = 5:1, **G$_2$**: SiO_2, AcOEt:C_6H_{14} = 1:3, **G$_3$**: SiO_2, CH_2Cl_2:C_6H_{14} = 5:1), and recrystallized (**G$_0$**: CH_2Cl_2, **G$_1$**: CH_2Cl_2, **G$_2$**: EtOH–Me_2CO, **G$_3$**: EtOH–Me_2CO).

G$_0$-QA: Yield 62 mg (87%); ^{1}H NMR ($CDCl_3$) δ 1.21 (s, 36H), 5.76 (s, 4H), 7.05 (s, 4H), 7.22 (t, J = 7.9 Hz, 2H), 7.32 (s, 2H), 7.42 (d, J = 7.9 Hz, 2H), 7.63 (t, J = 7.9 Hz, 2H), 8.52 (d, J = 7.9 Hz, 2H), 8.73 (s, 2H). Anal. Calcd for $C_{50}H_{56}N_2O_2$: C, 83.76; H, 7.87; N, 3.91%. Found: C, 83.64; H, 8.26; N, 3.60%.

G$_1$-QA: Yield 102 mg (74%); ^{1}H NMR ($CDCl_3$) δ 1.28 (s, 72H), 4.91 (s, 8H), 5.70 (br, 4H),* 6.53 (d, J = 1.8 Hz, 4H), 6.61 (t, J = 1.8 Hz, 2H), 7.21 (d, J = 1.7 Hz, 8H), 7.26 (t, J = 8.0 Hz, 2H), 7.36 (t, J = 1.7 Hz, 4H), 7.40 (d, J = 8.0 Hz, 2H), 7.65 (t, J = 8.0 Hz, 2H), 8.53 (d, J = 8.0 Hz, 2H), 8.71 (s, 2H). *The integration of this peak was observed to be 3.6H. Anal. Calcd for $C_{94}H_{112}N_2O_6$: C, 82.66; H, 8.26; N, 2.05%. Found: C, 82.76; H, 8.70; N, 1.85%.

G$_2$-QA: Yield 160 mg (60%); ^{1}H NMR ($CDCl_3$) δ 1.28 (s, 144H), 4.90 (s, 8H), 4.99 (s, 16H), 5.62 (br, 4H),* 6.45 (s, 4H), 6.55–6.57 (m, 6H), 6.63 (d, J = 1.7 Hz, 8H), 7.19 (t, J = 8.0 Hz, 2H), 7.25 (brs, 16H), 7.35 (d, J = 8.0 Hz, 2H), 7.38 (brs, 8H), 7.60 (t, J = 8.0 Hz, 2H), 8.50 (d, J = 8.0 Hz, 2H), 8.64 (s, 2H). *The integration of this peak was observed to be 1.4H. Anal. Calcd for $C_{182}H_{224}N_2O_{14}$: C, 82.06; H, 8.84; N, 1.05%. Found: C, 82.37; H, 9.02; N, 0.92%.

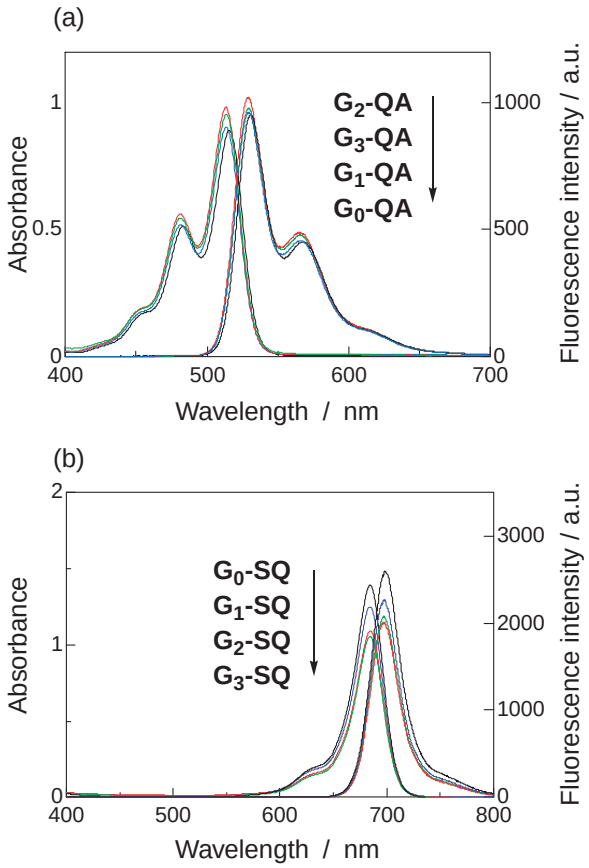

Fig. 3. UV–vis absorption and fluorescence spectra of **G_n-QAs** and **G_n-SQs**. In the case of **G_n-QAs**, UV–vis absorption spectra were measured at the concentration of 5×10^{-5} mol dm^{-3} in chloroform at 25 °C. The fluorescence spectra were measured in chloroform at the concentration of 1×10^{-5} mol dm^{-3} by irradiating 514 nm light. In the case of **G_n-SQs**, the UV–vis absorption spectra were measured at the concentration of 5×10^{-6} mol dm^{-3} in chloroform at 25 °C. The fluorescence spectra were measured at the concentration of 1×10^{-5} mol dm^{-3} of **G_n-SQs** by irradiating 684 nm light.

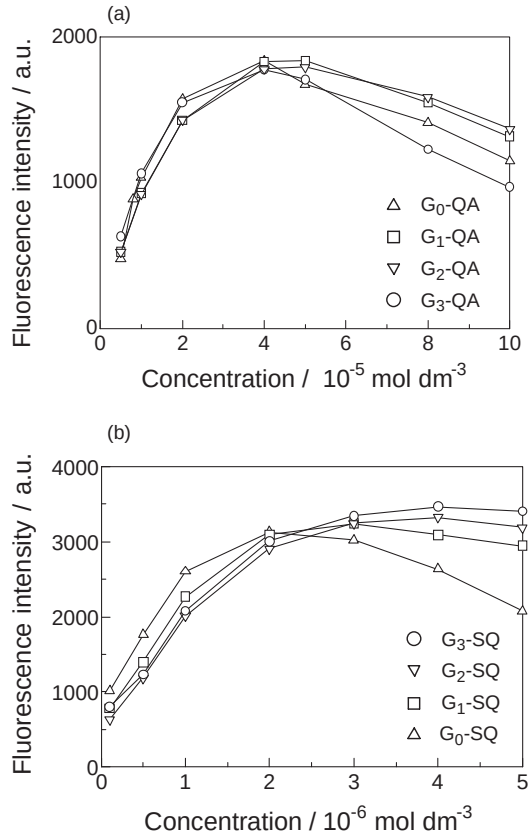

Fig. 4. Relationship between fluorescence intensity and concentration of **G_n-QAs** and **G_n-SQs**. In the case of **G_n-QAs**, fluorescence intensity was measured at 566 nm in chloroform. In the case of **G_n-SQs**, fluorescence intensity was measured at 697 nm in chloroform.

G_3-QA: Yield 94 mg (38%); ^{1}H NMR ($CDCl_3$) δ 1.27 (s, 288H), 4.90 (s, 24H), 4.97 (s, 32H), 6.44 (brs, 4H), 6.50 (brs, 4H), 6.56 (brs, 4H), 6.60 (brs, 8H), 6.62 (brs, 8H), 6.70 (brs, 16H), 7.14 (t, $J = 8.0$ Hz, 2H), 7.25 (brs, 32H), 7.31 (d, $J = 8.0$ Hz, 2H), 7.37 (brs, 16H), 7.55 (t, $J = 8.0$ Hz, 2H), 8.47 (d, $J = 8.0$ Hz, 2H), 8.62 (s, 2H). No peak assigned to four methylene-protons adjacent to benzothiazolyl-nitrogen was observed. Anal. Calcd for $C_{358}H_{448}N_2O_{30}$: C, 81.76; H, 8.59; N, 0.53%. Found: C, 81.17 H, 8.68; N, 0.39%.

Synthesis of Dihydroxysquarylium Dye (2). A butyl alcohol–benzene (4:1 v/v) mixed solution (20 cm^3) of 3-butyl-5-hydroxy-2-methylbenzothiazolium iodide (349 mg, 1 mmol), 3,4-dibutoxy-3-cyclobutene-1,2-dione (34 mg, 0.15 mmol), and quinoline (0.4 cm^3) was refluxed for 5 h. After cooling, the resulting precipitate was filtered and washed with hexane. Yield 47%; mp > 300 °C; ^{1}H NMR ($CDCl_3$) δ 0.94 (t, $J = 7.5$ Hz, 6H), 1.41 (sextet, $J = 7.5$ Hz, 4H), 1.66 (quintet, $J = 7.5$ Hz, 4H), 4.15 (t, $J = 7.5$ Hz, 4H), 5.72 (s, 2H), 6.72 (dd, $J = 8.0$ and 2.0 Hz, 2H), 6.86 (d, $J = 2.0$ Hz, 2H), 7.61 (d, $J = 8.3$ Hz, 2H), 9.92 (s, 2H).

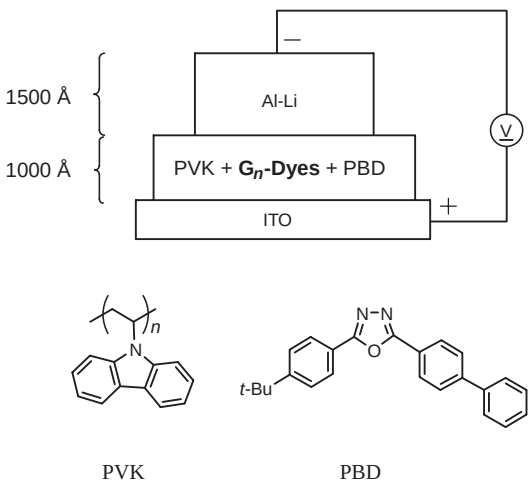

Fig. 5. EL device.

Synthesis of G_n-SQs. To DMSO (70 cm^3) were added the dihydroxysquarylium dye (**2**) (52 mg, 0.1 mmol), 18-crown-6-ether (16 mg, 0.06 mmol), and potassium carbonate (124 mg, 0.9 mmol). Then, the mixture was heated to dissolve all of the components. After cooling, **G_n-Br** (0.25 mmol) was added to the mixture, which was stirred for 4 h at room temperature under an argon atmosphere. After the reaction was completed, the mixture was poured into

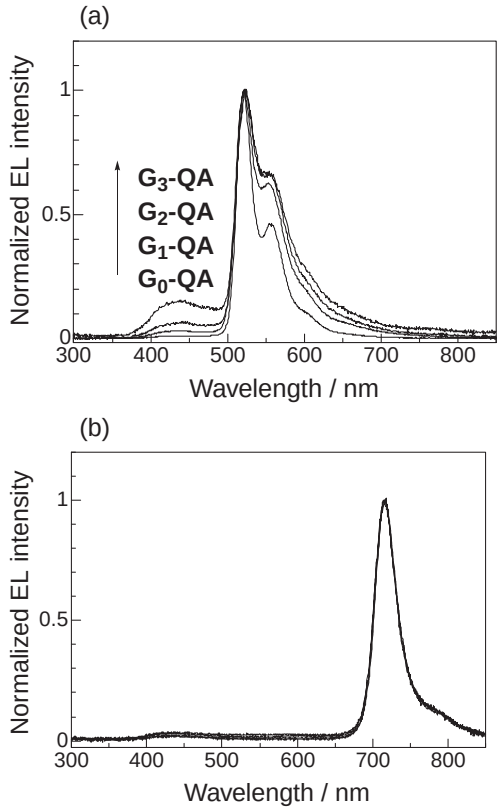

Fig. 6. EL spectra of (a) **G_n-QAs** and (b) **G_n-SQs**.

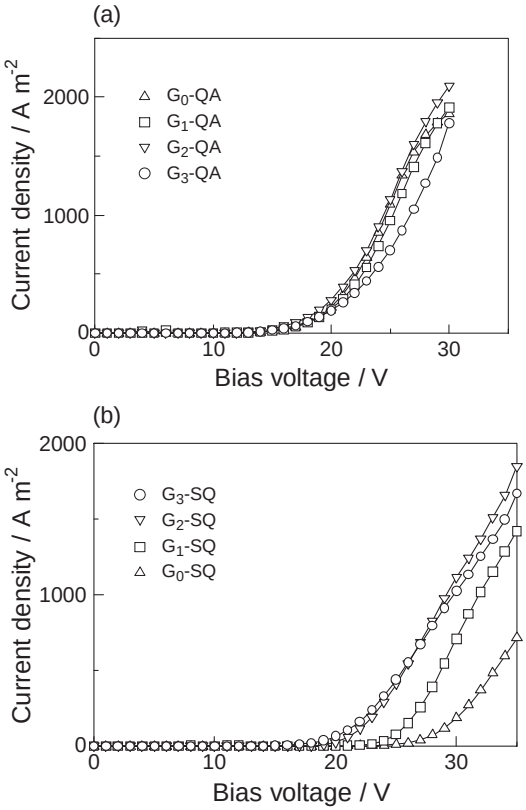

Fig. 8. Current density–voltage (I–V) characteristics of (a) **G_n-QAs** and (b) **G_n-SQs**.

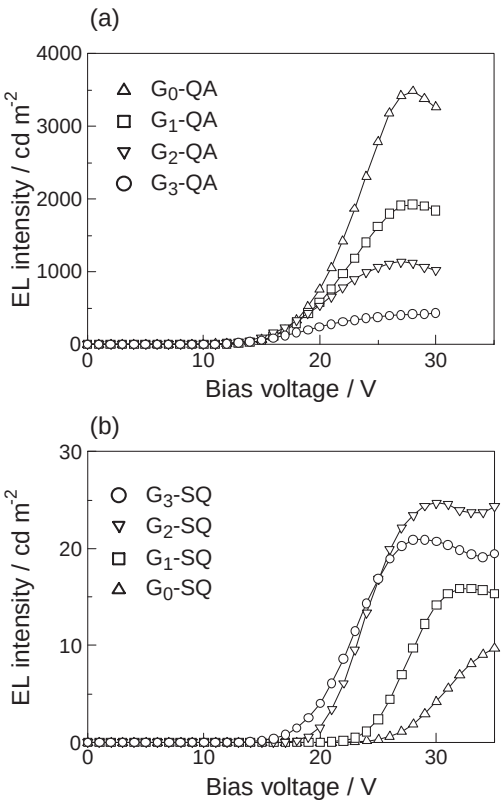

Fig. 7. Relationship between EL intensity and bias voltage in (a) **G_n-QAs** and (b) **G_n-SQs**.

water (50 cm^3). The product was extracted with dichloromethane (50 $cm^3 \times 3$) and purified by silica-gel chromatography (**G_0**: column, CH_2Cl_2:MeOH = 25:1, **G_1**: column, CH_2Cl_2:Me_2CO = 20:1, **G_2**: column, CH_2Cl_2:Me_2CO = 20:1, **G_3**, thin layer, CH_2Cl_2:Et_2O = 50:1). The physical and spectral data are shown below.

G_0-SQ: Yield 53 mg (57%); ^{1}H NMR ($CDCl_3$) δ 0.96 (t, J = 7.5 Hz, 6H), 1.33 (s, 36H), 1.40 (sextet, J = 7.5 Hz, 4H), 1.73 (quintet, J = 7.5 Hz, 4H), 3.97 (t, J = 7.5 Hz, 4H), 5.06 (s, 4H), 5.83 (s, 2H), 6.71 (d, J = 1.7 Hz, 2H), 6.87 (dd, J = 8.6 and 1.7 Hz, 2H), 7.26 (d, J = 1.7 Hz, 4H), 7.38 (d, J = 8.6 Hz, 2H), 7.42 (dd, J = 1.7 and 1.7 Hz, 2H). Anal. Calcd for $C_{58}H_{72}N_2O_4S_2$: C, 75.28; H, 7.84; N, 3.03%. Found: C, 74.62; H, 7.85; N, 2.93%.

G_1-SQ: Yield 107 mg (68%); ^{1}H NMR ($CDCl_3$) δ 0.96 (t, J = 7.5 Hz, 6H), 1.33 (s, 72H), 1.41 (sextet, J = 7.5 Hz, 4H), 1.72 (quintet, J = 7.5 Hz, 4H), 3.96 (t, J = 7.5 Hz, 4H), 5.00 (s, 8H), 5.06 (s, 4H), 5.83 (s, 2H), 6.65 (dd, J = 2.3 and 2.3 Hz, 2H), 6.70 (d, J = 2.3 Hz, 2H), 6.71 (d, J = 2.3 Hz, 4H), 6.82 (dd, J = 8.6 and 2.3 Hz, 2H), 7.27 (d, J = 1.7 Hz, 8H), 7.35 (d, J = 8.6 Hz, 2H), 7.41 (dd, J = 1.7 and 1.7 Hz, 4H). Anal. Calcd for $C_{102}H_{128}N_2O_8S_2$: C, 77.82; H, 8.20; N, 1.78%. Found: C, 77.79; H, 8.40; N, 1.72%.

G_2-SQ: Yield 105 mg (38%); ^{1}H NMR ($CDCl_3$) δ 0.96 (t, J = 7.5 Hz, 6H), 1.31 (s, 144H), 1.42 (sextet, J = 7.5 Hz, 4H), 1.76 (quintet, J = 7.5 Hz, 4H), 3.95 (t, J = 7.5 Hz, 4H), 5.00 (s, 24H), 5.03 (s, 4H), 5.83 (s, 2H), 6.61 (dd, J = 2.3 and 2.3 Hz, 2H), 6.65 (dd, J = 2.3 and 2.3 Hz, 4H), 6.67 (d, J = 2.3 Hz, 2H), 6.69 (d, J = 2.3 Hz, 4H), 6.71 (d, J = 2.3 Hz, 8H), 6.81 (dd, J = 8.6 and 2.3 Hz, 2H), 7.27 (d, J = 1.7 Hz, 16H), 7.35 (d, J = 8.6 Hz, 2H), 7.40 (dd, J = 1.7 and 1.7 Hz, 8H). Anal. Calcd for $C_{190}H_{240}$-

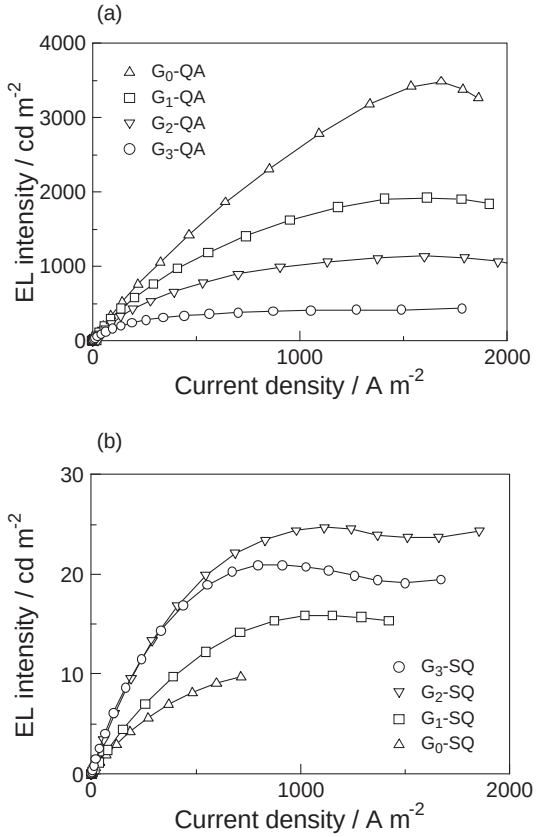

Fig. 9. Relationship between EL intensity and electron density of (a) **G_n-QAs** and (b) **G_n-SQs**.

$N_2O_{16}S_2$: C, 79.46; H, 8.43; N, 0.98%. Found: C, 79.62; H, 8.72; N, 0.98%.

G_3-SQ: Yield 120 mg (22%); ^{1}H NMR ($CDCl_3$) δ 0.97 (t, J = 7.5 Hz, 6H), 1.34 (s, 288H), 1.40–1.44 (m, 4H), 1.71–1.78 (m, 4H), 3.94–3.97 (m, 4H), 4.97–5.03 (m, 60H), 5.86 (s, 2H), 6.62–6.63 (m, 4H), 6.65 (brs, 2H), 6.66–6.67 (m, 8H), 6.71–6.72 (m, 14H), 6.74–6.75 (m, 16H), 6.83 (d, J = 8.6 Hz, 2H), 7.28 (brs, 32H), 7.36 (d, J = 8.6 Hz, 2H), 7.41 (brs, 16H). Anal. Calcd. for $C_{366}H_{464}N_2O_{32}S_2$: C, 80.40; H, 8.55; N, 0.51%. Found: C, 79.89; H, 8.68; N, 0.47%.

Solubility Measurement. A saturated solution of the substrate was prepared at 25 °C. The solution was filtered and diluted to measure the UV–vis absorption spectrum. The solubility was calculated on the basis of the known molar absorption coefficient in the solvent at the absorption maximum.

Fabrication of EL Device. ITO glass was sonicated in water, acetone, and isopropyl alcohol. Then, the glass was kept under an ozone atmosphere with UV irradiation. The ITO glass was used as the anode. To a toluene solution (3 cm^3) of poly(vinylcarbazole) (PVK) (40 mg) and 2-(4-biphenylyl)-5-(4-*t*-butylphenyl)-1,3,4-oxaziazole (PBD) (40 mg) was added **G_n-QA** (4.0×10^{-7} mol) or **G_n-SQ** (2.4×10^{-7} mol). The mixture was spin-coated (1000 rpm, 10 s then 2000 rpm, 10 s) on the ITO glass. The film thickness was adjusted to 1000 Å. Then, a cathode electrode of aluminum–lithium (99:1) alloy was prepared by vapor deposition method (0.5 nm s^{-1}). The EL device and the chemical structures of PVK, PBD, and **G_n-QAs** or **G_n-SQs** are shown in Fig. 5.

References

1 D.-L. Jiang, T. Aida, *Nature* **1997**, *388*, 454.
2 S. Yokoyama, A. Otomo, T. Nakahama, S. Mashiko, *Thin Solid Films* **2001**, *393*, 124.
3 D.-L. Jiang, T. Aida, *J. Am. Chem. Soc.* **1998**, *120*, 10895.
4 M. Brewis, G. J. Clarkson, V. Goddard, M. Heilliwell, A. M. Holder, N. B. McKeown, *Angew. Chem., Int. Ed.* **1998**, *37*, 1092.
5 P.-H. Liu, H. Tian, C.-P. Chang, *J. Photochem. Photobiol., A* **2000**, *137*, 99.
6 T. Wakimoto, T. Murayama, Jpn. Kokai Tokkyo Koho JP1993-70773, **1993**.
7 M. Nakatsuka, N. Kitamoto, Jpn. Kokai Tokkyo Koho JP11054283, **1999**; *Chem. Abstr.* **1999**, *130*, 202728.
8 H.-G. Kim, T. Mori, T. Mizutani, *T. IEE Jpn. E* **1998**, *118*, 223.
9 B. Zhang, W. Zhao, Y. Cao, X. Wang, Z. Zhang, X. Jiang, *Synth. Met.* **1997**, *91*, 237.
10 E. Horiguchi, T. Kitaguchi, M. Matsui, *Dyes Pigm.* **2006**, *70*, 43.
11 J. Qu, J. Zhang, A. C. Grimsdale, K. Müllen, F. Jaiser, X. Yang, D. Neher, *Macromolecules* **2004**, *37*, 8297.
12 P. Du, W.-H. Zhu, Y.-Q. Xie, F. Zhao, C.-F. Ku, Y. Cao, C.-P. Chang, H. Tian, *Macromolecules* **2004**, *37*, 4387.
13 A. W. Freeman, S. C. Koene, P. R. L. Malenfant, M. E. Thompson, J. M. J. Fréchet, *J. Am. Chem. Soc.* **2000**, *122*, 12385.
14 F. W. Zeng, S. C. Zimmerman, S. V. Kolotuchin, D. E. C. Reichert, Y. Ma, *Tetrahedron* **2002**, *58*, 825.
15 S. Yasui, M. Matsuoka, T. Kitao, *Dyes Pigm.* **1989**, *10*, 13.